# Using stellar scintillation for studies of turbulence in the Earth's atmosphere

Viktoria F. Sofieva, Francis Dalaudier, J. Vernin

PHILOSOPHICAL TRANSACTIONS OF THE ROYAL SOCIETY A

rsta.royalsocietypublishing.org

Review

**Cite this article:** Sofieva VF, Dalaudier F, Vernin J. 2013 Using stellar scintillation for studies of turbulence in the Earth's atmosphere. Phil Trans R Soc A 371: 20120174. http://dx.doi.org/10.1098/rsta.2012.0174

One contribution of 13 to a Theme Issue 'Turbulent mixing and beyond: non-equilibrium processes from atomistic to astrophysical scales I'.

**Subject Areas:**
atmospheric science, geophysics

**Keywords:**
stellar scintillation, atmosphere, turbulence, gravity waves, remote sensing

**Author for correspondence:**
V. F. Sofieva
e-mail: viktoria.sofieva@fmi.fi

Royal Society Publishing
*Informing the science of the future*

# Using stellar scintillation for studies of turbulence in the Earth's atmosphere

V. F. Sofieva[1], F. Dalaudier[2] and J. Vernin[3]

[1]Finnish Meteorological Institute, PO Box 503, 00101 Helsinki, Finland
[2]LATMOS IPSL, CNRS/INSU, Université Versailles St-Quentin, UPMC Université Paris 06, 78280 Guyancourt, France
[3]Laboratoire Lagrange, CNRS UMR7293, Observatoire de la Côte d'Azur, Université de Nice – Sophia Antipolis, 06108 Nice 2, France

Stellar scintillation observed through the Earth's atmosphere is the result of interaction of light waves and the turbulent atmosphere. This review is dedicated to using stellar scintillation measurements for studies of turbulence in the Earth's atmosphere. We present an overview of ground-based, airborne and satellite stellar scintillation measurements, discuss the approaches to data analyses and give an overview of the main geophysical results. We also discuss the benefits of the scintillation method in studies of the structure of air density irregularities and its limitations.

## 1. Introduction

Ages ago observers noticed twinkling of stars in the night sky. Twinkling stars have been a source of inspiration for many artists and astronomers. While artists have created beautiful paintings and poetry, astronomers have been inspired to understand the causes of the twinkling and how to eliminate it. In science, the technical term 'scintillation' is used for the twinkling of stars.

It took a long time to understand the true reason for twinkling of stars. First theories by Aristotle [1] and Ptolemy attributed twinkling of stars to a weakness of human vision. They assumed that seeing is related to some human flux going from the eye to the target. The farther the target, the stronger the scintillation, and, as a consequence, planets are twinkling less than stars. Leonardo da Vinci also believed that the reason for stellar scintillation belongs to the human eye and is an optical illusion [2]. In the late sixteenth century,

Tycho Brahe related twinkling of stars to the movement of the stars in the celestial sphere, while Johannes Kepler believed that stellar scintillation is caused by actual changes in the brightness and colour of the stars [3]. It was Isaac Newton who first found, in the early eighteenth century, the true cause of stellar scintillation. He realized that atmospheric turbulence is responsible for the twinkling of the stars [4]. In the nineteenth century, scintillation studies entered a new phase and obtained scientific interpretation thanks to the works and observations by Arago [5], Donati [6], Dufour [7], Montigny [8–10], Wolf [11] and Respighi [12].

It is well known nowadays that scintillation of stars is the result of interaction of stellar light and air density (and, consequently, refractive index) irregularities. In a simplified qualitative explanation, scintillation can be considered as random focusing and defocusing of stellar light. This phenomenon is analogous to the light pattern at the bottom of a sun-lit swimming-pool. The theory of stellar scintillation and its relationship with atmospheric turbulence has been a subject of intensive research.

This review is dedicated to using stellar scintillation for studies of atmospheric turbulence. By 'turbulence', we mean any kind of fluctuations that are responsible for the observed scintillations. These include mostly usual turbulence (isotropic, strongly nonlinear) and gravity waves (GWs; strongly anisotropic and weakly nonlinear); other kinds of fluctuations can also be present. We restrict the scope of this review to consider the scintillation of stars only (while there are also scintillations of planets, radio sources and even interstellar scintillation of radio waves) with application to the Earth's atmosphere only (although the technique can also be applied to the atmosphere's of other planets, either from an orbit around the planet, or from the Earth). We present an overview of ground-based, air-borne and satellite stellar scintillation measurements in the Earth's atmosphere, discuss the approaches to data analyses aimed at quantifying the parameters of atmospheric turbulence, and give an overview of the main geophysical results.

## 2. Atmospheric sources of scintillation

Scintillation is the result of interaction of a light wave with atmospheric air density irregularities. The atmosphere is a complicated fluid: it is stably stratified but nearly everywhere (and always) at the border of instability. It contains a broad range of scales and a broad range of physical phenomena, most of which are nonlinear. It is anisotropic, inhomogeneous and non-stationary. Small-scale air density irregularities, which cause the observed scintillations, are produced by turbulence, internal GWs and instabilities of different kinds.

In the stochastic description of turbulence, the atmosphere is described as a base state with superimposed fluctuations. The fluctuations are assumed to possess the nature of a stochastic field. The base state of the atmosphere is close to some steady state (this is common for 'natural' phenomena). The fluctuations mainly result from instabilities in this steady state or instabilities in the 'perturbations' of this steady state (such as GWs). Furthermore, the long-term action of the perturbations can affect the base state.

Atmospheric air density fluctuations define a random field of relative fluctuations of refractivity $\nu = (N - \langle N \rangle)/\langle N \rangle$ (here $N = n - 1$ is refractivity, $n$ is the refractive index, and angular brackets hereafter denote the statistical mean). For 'optical' wavelengths, $0.2 < \lambda < 20\,\mu\text{m}$, the mean refractivity is defined by

$$\langle N(h) \rangle = 77.6 \times 10^{-6} \frac{\langle P(h) \rangle}{\langle T(h) \rangle} \left( 1 + \left( \frac{\Lambda}{\lambda} \right)^2 \right), \tag{2.1}$$

where $\langle T(h) \rangle$ (K) and $\langle P(h) \rangle$ (hPa) are atmospheric temperature and pressure profiles, $\lambda$ (nm) is the wavelength of light and the parameter $\Lambda = 87\,\text{nm}$ describes the optical dispersion of air. Equation (2.1) shows that refractivity is proportional to air density and depends weakly on the wavelength. The wavelength variations are mainly in the UV part of the spectrum: $[\nu(300\,\text{nm}) - \nu(400\,\text{nm})]/\nu(300\,\text{nm}) \approx 3\%$, while $[\nu(1300\,\text{nm}) - \nu(1400\,\text{nm})]/\nu(1300\,\text{nm}) \approx 0.046\%$. There also exist more accurate analogues of equation (2.1) [13,14]. Assuming the base state of the atmosphere

to be very close to hydrostatic equilibrium, the refractivity fluctuations can be considered proportional to temperature fluctuations: $\nu = -\delta T/\langle T\rangle$. This implies that relative fluctuations of pressure are vanishing.

In general, the field of refractivity fluctuations is described by random functions of three spatial coordinates (or the spatial vector $\mathbf{r} = (x, y, z)$, $z$ being the vertical coordinate) and time. However, for application to scintillations, the turbulence can be considered as 'frozen', as it is observed by a sensor (Taylor's frozen-field approximation). This allows consideration of the random field depending on the spatial component only. The random refractivity field is assumed to be locally homogeneous, which is the spatial equivalent of a random process with stationary increments. Locally homogeneous fields are characterized usually by the structure function:

$$D_\nu(\mathbf{r}) = D_\nu(\mathbf{r}_1 - \mathbf{r}_2) = \langle(\nu(\mathbf{r}_1) - \nu(\mathbf{r}_2))^2\rangle, \tag{2.2}$$

where $\mathbf{r}_1$ and $\mathbf{r}_2$ are two locations and $\mathbf{r} = \mathbf{r}_1 - \mathbf{r}_2$. The spectral representation of the structure function is [15]

$$D(\mathbf{r}) = 2\int \mathrm{d}^3\boldsymbol{\kappa}\, \Phi(\boldsymbol{\kappa})(1 - \cos(\boldsymbol{\kappa}\mathbf{r})), \tag{2.3}$$

where $\Phi(\boldsymbol{\kappa})$ is the spatial three-dimensional spectrum, and $\boldsymbol{\kappa} = \{\kappa_x, \kappa_y, \kappa_z\}$ is the wavevector.

If the field of refractivity fluctuations is assumed to be locally isotropic [15,16], $\Phi(\boldsymbol{\kappa})$ in this model can be written as

$$\Phi(\boldsymbol{\kappa}) = C_n^2|\boldsymbol{\kappa}|^{-\mu} = C_n^2(\kappa_\perp^2 + \kappa_z^2)^{-\mu/2}, \quad \kappa_\perp^2 = \kappa_x^2 + \kappa_y^2, \quad \kappa^2 = \kappa_\perp^2 + \kappa_z^2, \quad \kappa_* < \kappa < \kappa_m, \tag{2.4}$$

where $C_n^2$ is the structure characteristic, and $2\pi/\kappa_*$ and $2\pi/\kappa_m$ are outer and inner scales, respectively. To account for the influence of the inner scale on the spectrum, one can multiply (2.4) by a function $f(\kappa/\kappa_m)$, which is close to 1 for $\kappa/\kappa_m = 1$ and approaches 0 for $\kappa/\kappa_m = 1$. The spectrum (2.4) has a constant value on the spherical surface with radius equal to $|\boldsymbol{\kappa}|$. The model (2.4) with $\mu = -11/3$ corresponds to the Kolmogorov spectrum [15] with one-dimensional spatial spectrum of $V(|\boldsymbol{\kappa}|)$ and the structure function $D(|\mathbf{r}|)$ in the inertial sub-range $\kappa_* < |\boldsymbol{\kappa}| < \kappa_m$:

$$V(|\boldsymbol{\kappa}|) \sim C_n^2|\boldsymbol{\kappa}|^{-5/3} \quad \text{and} \quad D(|\mathbf{r}|) = C_n^2\,|\mathbf{r}|^{2/3}. \tag{2.5}$$

For the atmosphere, the inner scale $1/\kappa_m$ is proportional to the Kolmogorov scale $l_\mathrm{K} = \nu_\mathrm{a}^{3/4}\varepsilon^{-1/4}$, where $\varepsilon$ is the kinetic energy dissipation rate and $\nu_\mathrm{a}$ is the molecular kinematic viscosity for air. Numerous observations in the boundary layer of the atmosphere have shown an excellent agreement of the measurements with model (2.5) under the conditions of unstable or neutral temperature stratifications (e.g. [15,17] and references therein; [18]).

The model (2.4) assumes that all directions in the turbulent atmosphere are treated equally. This assumption is justified if the influence of the buoyancy forces on the formation of refractivity irregularities can be neglected. Under the conditions of stable temperature stratification with a low gradient of wind speed, for example, such an assumption cannot be valid. Local vertical becomes a distinguished direction. The simplest way to adjust the spectrum $\Phi_n(\boldsymbol{\kappa})$ to the presence of a distinguished direction is to introduce the notion of the anisotropy coefficient $\eta$ [16]. As a result, the three-dimensional spectrum and the structure function take the following forms:

$$\left.\begin{aligned} &\Phi_n(\boldsymbol{\kappa}) = \eta^2 C_n^2(\kappa_\perp^2\eta^2 + \kappa_z^2)^{-\mu/2}, \quad 3 < \mu < 5 \\ \text{and} \quad &D_n(\mathbf{r}) \sim C_n^2\left(\frac{x^2 + y^2}{\eta^2} + z^2\right)^{(\mu-3)/2}, \quad \eta \geq 1. \end{aligned}\right\} \tag{2.6}$$

Spectrum (2.6) is derived from (2.4) by a scaling operation. The aspect ratio of the ellipsoid $D_n(\mathbf{r}) = \text{const.}$ equals $\eta$. The anisotropy coefficient $\eta$ represents here the ratio of horizontal to vertical scales: $D_n(\sqrt{x^2 + y^2}) = D_n(\eta z)$, $\eta^2 z^2 = x^2 + y^2$. Both vertical and horizontal one-dimensional spectra in model (2.6) follow the same $-\mu + 2$ power law. A three-dimensional spectrum analogous to (2.6) with $\mu = 5$, where the wavenumbers $\kappa_0$ and $\kappa_W$ and corresponding outer ($L_0 = 2\pi/\kappa_0$) and inner ($l_W = 2\pi/\kappa_W$) is observed scales are introduced, has been used

in [19,20] for interpretation of scintillation spectra caused by anisotropic irregularities of air density observed from satellites:

$$\Phi_W = C_W \eta^2 (\kappa_z^2 + \eta^2 \kappa_\perp^2 + \kappa_0^2)^{-5/2} f\left(\frac{\kappa}{\kappa_W}\right). \tag{2.7}$$

In (2.7), $C_W$ is the structure characteristic. The spectrum (2.7) but without the outer scale has been used in [21] for characterization of the anisotropic component of scintillation spectra observed from the AMON-RA experiment. The choice of the slope $-5$ is dictated by the condition for the one-dimensional vertical wavenumber spectrum to follow $\kappa_z^{-3}$ for $\kappa_0 < \kappa < \kappa_W$. This corresponds to the model of saturated GWs [22] for the one-dimensional vertical spectrum of relative temperature fluctuations:

$$V_{\delta T/T} = A \frac{\omega_{\mathrm{BV}}^4}{g^2} \kappa_z^{-3}, \tag{2.8}$$

where $\omega_{\mathrm{BV}}$ is the local Brunt–Väisälä frequency, $g$ the acceleration due to gravity and $A$ is a numerical coefficient. For $A = 0.1$–$0.3$, equation (2.8) is consistent with the experimental data thoroughly reviewed in [23]. This power-law decay for the three-dimensional spectrum follows also from the theoretical model of an internal GW spectrum [19]. The parameter $\eta$ in (2.7) is constant, i.e. it does not depend on the scale of irregularities.

A model for the spatial three-dimensional spectrum of temperature irregularities generated by internal GWs, which originate and propagate in a stably stratified atmosphere, was suggested in [24]. This is also a model with constant anisotropy, which gives the same power law for the corresponding one-dimensional vertical and horizontal wavenumber spectra.

However, systematic measurements [25–27] have shown that the horizontal spectra are close to a $\kappa_y^{-5/3}$ dependence over a large interval of wavenumbers. To account for different slopes of one-dimensional vertical and horizontal spectra, a model with variable anisotropy was proposed in [28]. This model develops the ideas discussed in [29,30]. The ratio of the horizontal and vertical scales—that is, the anisotropy coefficient $\eta$—characterizes the shape of the irregularities. The anisotropy coefficient is larger than one, $\eta \geq 1$, and increasing with the vertical scale of irregularities. In [28], it is suggested that $\eta$ depends only on the vertical scale of irregularities: $\eta = \eta(\kappa_z/\kappa_w)$, where $2\pi/\kappa_w$ is some characteristic scale of transition towards isotropy. The authors have proposed a model of the three-dimensional spectrum of temperature irregularities [28]. The one-dimensional vertical spectrum corresponding to this model behaves as $\sim \kappa_z^{-3}$, while, if one assumes $\eta \sim (\kappa_w/\kappa_z)^2$, the horizontal spectrum has the slope $-5/3$ over a wide range of wavenumbers, which agrees with observations. Although more accurate, the models with variable anisotropy have not yet been used for interpretations of scintillation measurements (see also the discussion in §5*e*).

Although there exist models of the three-dimensional spectrum of atmospheric irregularities that have been successfully used for interpretation of scintillation measurements, the small-scale structure of atmospheric irregularities is very complex and still incompletely described. Measurements of the atmospheric microstructure reveal a fairly large number of very strong (positive) temperature gradients (approx. 30–100 $\mathrm{K\,km^{-1}}$) within very thin layers (approx. 3–20 m). Such data are obtained with fast-response temperature sensors on balloons, radar echoes and scintillations of binary stars [31–34]. The 'sheets' are observed at various altitudes, most of them being in the lower stratosphere. *In situ* measurements with sensors some distance apart show that the 'sheets' are neither flat nor horizontal. Mixing within these thin layers has been detected [33,35]. Other relatively recent analyses apply multifractal models to describe the atmospheric structure [36,37]. For a review of these analyses and the resulting space–time cascade model, which is based on strongly anisotropic and intermittent generalizations of the classical turbulence laws, see [38]. Spatial inhomogeneity and intermittency (the atmosphere is not everywhere and not always turbulent; when turbulent, the parameters change from region to region) introduce further complication into the description of atmospheric turbulence.

The theory of turbulence in stably stratified media is still under development and is the subject of active discussions. Intensive work is being done towards the development of new turbulence closure theory [39–41] and the quasinormal scale elimination model [42–44].

## 3. Theory of scintillation

The general theory of scintillation for ground-based and spacecraft observations was developed by Tatarskii [15] and Ishimaru [16]. Stars can be considered as point sources of light, and wavefronts can be assumed to be a plane at the entrance of the atmosphere. Atmospheric irregularities have a random structure, producing random effects on stellar light that passes through the atmosphere. These require a statistical description, by either autocorrelation functions, spatial wavenumber spectra or structure functions. These descriptions are integral transforms of one another, thus being equivalent in some sense. Theoretical approaches relate the characteristics of a model of the turbulent medium and the observed scintillations. They have been developed for both wave-optical treatment and geometrical-optics approximation, using the power spectrum of refractive-index fluctuations or corresponding structure functions. A number of monographs exist on wave propagation in random media: classical ones by Tatarskii [15,45], as well as [16,46–48]. A general theory of scintillation observed from space is developed in [16,49–52]. The phenomena associated with star scintillation as observed from the ground was reviewed by Dravins *et al.* in three papers [53–55].

As was mentioned above, the frozen-field hypothesis is used for describing scintillation phenomena. Within the Rytov smooth perturbation approximation [47], there is a fairly simple connection between the (three-dimensional) spectrum of refractive index fluctuations and the two-dimensional scintillation spectrum in the observation plane. So far, these relations have been used to retrieve the parameters of the spatial spectrum of refractive index fluctuations from satellite and *in situ* scintillation measurements [19–21,56–58]. The Rytov method is valid when the monochromatic scintillation variance $\sigma_I^2 = \langle (I - \langle I \rangle)^2 / \langle I \rangle^2 \rangle$ is small, $\sigma_I^2 \ll 1$ (weak fluctuations). For more general conditions (strong scintillations), the moment equations are so difficult that they are solved only for some special cases and approximations. A variety of techniques have been proposed such as the parabolic equation method [16,59], extended Huygens–Fresnel principle [16,60], multiple phase screen [61], the path integral [62,63] and numerical techniques [64,65]. Among these, the parabolic equation method with the Markov approximation [59,66] occupies an important place.

The theory of strong scintillations applied to the stellar occultation measurements has been further developed by Gurvich *et al.* [67]. That paper considers the problem of remote sensing of stratospheric irregularities under strong scintillation conditions. The authors have analysed calculated scintillation spectra and have concluded that the parameters of the three-dimensional spectra of stratospheric irregularities can be retrieved under the conditions of relatively strong scintillation (characterized by scintillation variance computed with weak fluctuation assumption below 1.5–1.6).

Since the scintillation theory is based on the theory of wave propagation in random media, several studies have been dedicated to checking its validity. In particular, the probability density function of scintillations has been examined. Weak perturbation theory predicts starlight to be lognormally distributed, as the refractive-index fluctuations, which can be considered as a large number of independent events, modulate the intensity in a multiplicative manner. For small and moderate scintillation amplitudes, the experimental distributions follow the lognormal law, but for greater ones, departures occur, as expected [21,53,68].

The scintillation method, as a tool for studying atmospheric turbulence, has specific features and limitations. First, scintillation measurements are not direct: in order to get information about small-scale processes, a functional relationship between the equivalent parameters of atmospheric irregularities and parameters of observed scintillation or solution of the inverse problem is needed. Conceptually, the problem is simpler in two dimensions, but observations are mostly one-dimensional. The amount of all currently available scintillation measurements is not sufficient for reconstructing the structure of air density via solving the tomography problem (as described, for example, in [69]). Instead, spectral properties of atmospheric irregularities are assumed, so that a relationship between the structure of air density irregularities and the parameters of the observed scintillations can be found. Second, depending on the measurements, scintillations are insensitive

to some parameters of the atmospheric spectral model. This is discussed in more detail in sections dedicated to particular types of measurements. Third, the parameters of the spectral model ($C_n^2$, for instance) estimated from scintillation measurements represent 'effective' parameters averaged along a ray with the weight function determining the effective region of interaction between the light wave and the turbulent atmosphere. Fourth, the smallest scale observable from scintillation is the diffractive Fresnel scale, $Fr = \sqrt{\lambda L/2\pi}$, where $L$ is the distance from the observer to the point representing the interaction region of the light wave and the turbulent atmosphere.

For recording scintillations, important are star magnitude and the size of the telescope (in order to get sufficient signal-to-noise ratio), the sampling rate of the detector (in order to get sufficient resolution) and the chromatic width of the optical filter (chromatic refraction in the atmosphere leads to changes in the bandwidth scintillation spectrum, particularly, to attenuation of variance).

The specifics of data, processing and retrieved parameters depend on the geometry of line of sight. In the following, we review the data processing and the results from ground-based, satellite and air-borne measurements of stellar scintillation.

# 4. Ground-based measurements of stellar scintillation

## (a) Introductory notes

Quantitatively, scintillation observed on the ground can be explained as follows. Let us imagine one optical turbulent layer moving at altitude $h$ above the ground, as sketched in figure 1. After passing through the turbulent layer, the wavefront, which was initially a plane, becomes distorted. Light rays propagate perpendicularly to the wavefront towards the ground, converging in some places and diverging in others, giving rise to bright and dark speckles. It is important to recall that scintillation is related to light intensity fluctuations and not to phase or complex amplitude. In figure 1, if one puts one's eye, or a photoelectric receiver, just after the turbulent layer, one will see the star wandering, if the eye pupil is less than the spatial coherence of the wavefront. The receiver will not yet notice any intensity variation, because light rays do not have enough propagation space after crossing the turbulent layer. At ground level, after propagation over a distance $h$, light beams converge and diverge to produce speckle patterns, known as 'shadow band patterns'. This is well described in [45,70] in the framework of Fresnel diffraction.

For ground observations, where the line of sight is nearly vertical, the strongly anisotropic fluctuations (generated mostly by GWs) can be completely ignored. The reason for the elimination of the anisotropic component is that scintillation results from refractivity gradients perpendicular to the line of sight. Because of the rather large horizontal scales of the GW component (many kilometres) and of its very large anisotropy, the corresponding gradients can be ignored completely; thus turbulence can be regarded as isotropic (or nearly so). Furthermore, because of the strong anisotropy, this approximation is valid up to large angles from the vertical (as large as approx. 75°), thus covering all the astronomical applications. In analyses of ground-based stellar scintillation measurements, the Kolmogorov spectrum is assumed.

## (b) Multi-dimensional scintillation analysis

Since the 1960s, most scintillation studies have been performed on one-dimensional temporal signals $I(t)$, which reflect all the perturbations from the whole atmosphere. Even if one makes the stationary assumption along with the frozen turbulence hypothesis, there is no way to retrieve detailed vertical profiles of turbulence from the temporal autocorrelation of the scintillation observed at the ground. This is because of the fact that the atmosphere is never moving as a whole with a constant velocity. Hence, the ground intensity is the superposition of many scintillation patterns from turbulent layers moving at various velocities in different directions. A few attempts have been made to obtain spatial power spectra using different spatial filtering in the pupil plane [71–73]. Measurements by Protheroe [72] agreed well with a layer propagating at an altitude

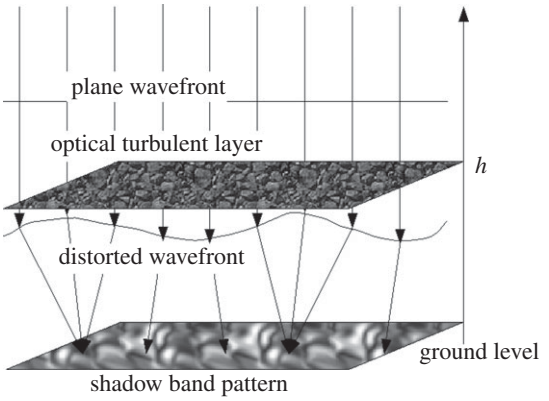


**Figure 1.** Light propagation through an optical turbulent layer. Wavefront is assumed to be a plane on top of our atmosphere and then crosses a turbulent medium where it is bent by refractive index fluctuations. Just after passing through the turbulent layer, light rays are dangling perpendicularly to the wavefront, but no intensity fluctuation is detected. At the ground level, the light beam converges and diverges to create bright and dark speckles, i.e. stellar scintillation.

of approximately 10 km. Owing to the above-mentioned superposition of many layers, neither the fine structure of the atmosphere nor any information about the ground layer is attainable.

The idea of using a 'multi-dimensional analysis' of the scintillation in order to obtain information about the layered structure of the atmosphere has been proposed in [31,74,75]. In this approach, the scintillation intensity $I$ is considered as a multi-dimensional function of time, wavelength $\lambda$, position of the observer $\mathbf{r}(x, y)$ and angular position of the star $(\alpha, \beta)$:

$$I = I(t, \lambda, x, y, \alpha, \beta). \tag{4.1}$$

By finding the cross-correlation function of scintillation with respect to several of these variables, it is possible to retrieve the turbulence parameters corresponding to different layers with different $C_n^2$ and different velocities $\mathbf{v}$. For example, the spatio-wavelength analysis allows optical turbulence profiles to be retrieved (§4*b*(i)). The spatio-angular technique, first developed by Rocca *et al.* [74] and then by Vernin & Roddier [75], has opened the era of the Scidar (scintillation and ranging, by analogy with radar) technique, which has become a standard tool for remote sensing of the Earth's atmosphere. This method is discussed in §4*b*(ii). The 'generalized Scidar' technique (§4*b*(iii)) allows the optical turbulence also at the ground level to be detected. The spatio-temporal technique constitutes the basis for data analyses using the so-called single star Scidar (SSS); this is discussed more in §4*b*(iv).

### (i) Spatio-wavelength analysis: the differential refraction

The spatio-wavelength analysis can be applied for bright stars close to the horizon, as was demonstrated by Caccia *et al.* [76]. When stars are approaching the horizon, scintillation becomes chromatic. This phenomenon is related to the refractive index dependence on wavelength, thus resulting in different bending. A cut of the cross-correlation of the scintillation pattern at $\lambda_1$ and $\lambda_2$, $C_I(0, y, \lambda_1 - \lambda_2) = \langle I(0, y', \lambda_1) I(0, y' + y, \lambda_2) \rangle$, assuming that the $y$-axis is perpendicular to the horizon, allows us to retrieve vertical profiles of optical turbulence. Since this experiment works only with very bright stars (Sirius) close to the horizon, the method was abandoned.

### (ii) Spatio-angular analysis: the Scidar

The Scidar principle (figure 2*a*) was first proposed by Rocca *et al.* [77]. Two stars separated by an angle $\theta$ cast onto the ground two identical speckle patterns (or scintillation), but displaced from one another by a distance $d = \theta h$, $h$ being the altitude of the layer. The distance $d$ is

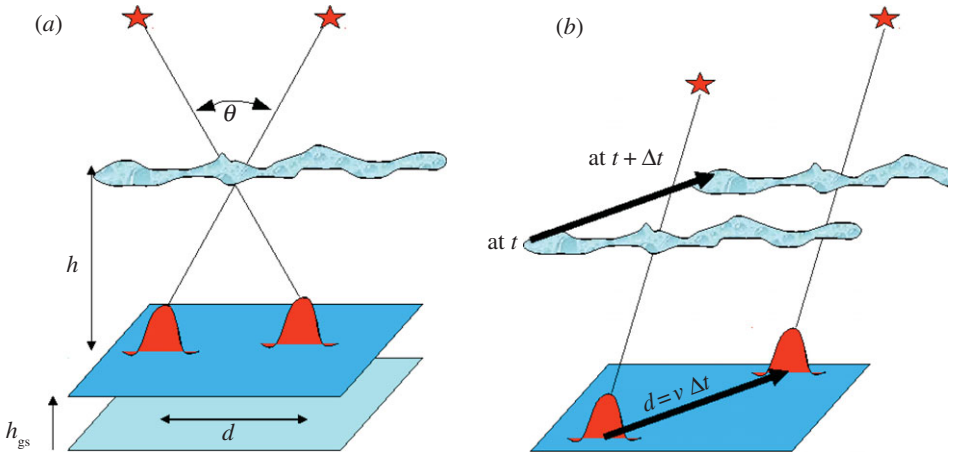


**Figure 2.** (*a*) Principle of the Scidar technique: two stars cast two scintillation patterns onto the ground separated by $d = \theta h$. (*b*) Principle of the SSS technique: a single star casts two scintillation patterns at different temporal sampling onto the ground, separated by $d = v\,\Delta t$. (Online version in colour.)

measured by computing the autocorrelation function of the scintillation patterns, which peaks at $d$. The intensity of the peak is related to the refractive index structure characteristic $C_n^2(h)$. Each turbulent layer produces a bump in the measured autocorrelation function (since the width of the autocorrelation function is proportional to the Fresnel scale, the higher the layer, the wider the bump).

For a continuous distribution of turbulent layers, the relationship between the measured autocorrelation function of the scintillation produced by a double star $C_{**}(\mathbf{r})$ and the $C_n^2(h)$ distribution is

$$C_{**}(\mathbf{r}) = \int_0^\infty \mathrm{d}h\, C_n^2(h)\{aC_*(\mathbf{r},h) + b[C_*(\mathbf{r}-\boldsymbol{\theta}h,h) + C_*(\mathbf{r}+\boldsymbol{\theta}h,h)]\}, \tag{4.2}$$

where $C_*(\mathbf{r},h)$ is the autocorrelation function of the scintillation produced by a single star and a layer at altitude $h$, and $a$ and $b$ are related to the magnitude difference $\Delta m$ between each component of the double star:

$$\alpha = 10^{-0.4\Delta m}, \quad a = \frac{1+\alpha^2}{(1+\alpha)^2} \quad \text{and} \quad b = \frac{\alpha}{(1+\alpha)^2}. \tag{4.3}$$

Equation (4.2) is an integral relationship between $C_{**}(\mathbf{r})$ and $C_n^2(h)$ with the kernel $K = aC_*(\mathbf{r},h) + b[C_*(\mathbf{r}-\boldsymbol{\theta}h,h) + C_*(\mathbf{r}+\boldsymbol{\theta}h,h)]$. Avila *et al.* [78] first mentioned the use of the maximum entropy method to invert this relationship and retrieve the $C_n^2$ profile.

### (iii) The generalized Scidar

The Scidar experiment was tested in many observatories and validated with comprehensive comparisons with other techniques such as a Differential Image Motion Monitor (DIMM) and instrumented balloons measuring the optical turbulence [79]. In its classical version, the Scidar is still insensitive to low-layer turbulence, which can largely affect the astronomical seeing (or image degradation) within a 50–80% proportion.

Fuchs *et al.* [80] first proposed analysing the scintillation in a virtual plane, below the pupil plane by a distance $h_{gs}$, as sketched in figure 2*a*. This plane disposition allows a layer at ground altitude to have enough Fresnel propagation to give scintillation, because $h_{gs} \neq 0$. Using a laboratory demonstrator, these authors have shown that the variance of the scintillation was positive when a phase screen (turbulent layer) was close to the pupil plane, goes to zero

at a distance $h = h_{gs}$ (gs for generalized Scidar), and then increases again at larger distances. Equation (4.2) is changed to

$$C_{**}(\mathbf{r}) = \int_0^\infty \mathrm{d}h\, C_n^2(h)\{aC_*(\mathbf{r}, H) + b[C_*(\mathbf{r} - \boldsymbol{\theta}H, H) + C_*(\mathbf{r} + \boldsymbol{\theta}H, H)]\}, \tag{4.4}$$

where $H = h - h_{gs}$ and $h_{gs}$ is the virtual altitude in the generalized Scidar mode. This altitude, which increases the Fresnel propagation distance, needs to be larger than zero but sufficiently low in order to avoid a saturation effect of the scintillation variance.

The generalized Scidar became a standard instrument for remote sensing of the atmosphere for astronomical purposes as well as for atmospheric studies. There still remains a strong restriction on the size of the entrance pupil of the telescope, $D_{\text{telescope}}$, which needs to be larger than $\theta h_{\max}$, $h_{\max}$ being the maximum altitude that one wants to sample. Generally, for available bright double stars with a small difference in magnitude $\Delta m$, one needs a 1.5 m telescope, which limits the use of the Scidar to existing observatories already equipped with large telescopes.

### (iv) Spatio-temporal analysis: the single star Scidar

The spatio-temporal analysis, i.e. the analyses of the auto- and cross-correlation of time evolution of scintillation,

$$\Gamma_*(x, y, \tau) = \langle I(x', y', t) I(x' + x, y' + y, t + \tau)\rangle, \tag{4.5}$$

has found its application in the so-called SSS technique [74,81–84]. Figure 2*b* shows the SSS principle for a single turbulent layer. In the real atmosphere, many layers are moving at different velocities $\mathbf{v}_i$ leading to many cross-correlation peaks situated at $\mathbf{d}_i = \mathbf{v}_i\tau$. One might think that a simple cross-correlation function $\Gamma_*(x, y, \tau)$ should be sufficient to retrieve $C_n^2(h)\delta h$ and $\mathbf{v}(h)$ related to each turbulent layer: the position of the bump giving the velocity, its amplitude giving $C_n^2(h)\delta h$ and the size of the bump giving the altitude of the layer through its proportionality to the Fresnel scale. However, Caccia & Vernin [84] have demonstrated that the latter assumption is not true, because the dispersion of the wind velocity $\sigma_v$ enlarges the size of the cross-correlation peak. This can be described as a convolution of the natural correlation by a Gaussian function whose width is proportional to the time lag $\tau$. Since the decorrelation due to velocity dispersion does not have the same effect on the enlargement of the autocorrelation as that due to altitude ($\sqrt{\lambda h}$), the inversion is possible only if the cross-correlation is measured at various lags. The inversion is an ill-posed problem, which can be solved, for example, with the simulated annealing technique [85].

The SSS concept was validated in several places before being sent to Dome C on the high Antarctic plateau, where routine observations have been performed during 2006 and 2007 polar nights. The instrument is made of a portable 40 cm telescope, an optical bench with a stop field and a 10 mm collimating lens and a fast readout charge-coupled device (CCD) camera. Under clear sky conditions, vertical profiles of $C_n^2(h)$, velocity components $v_x(h)$ and $v_y(h)$, and the wind velocity dispersion $\sigma_v(h)$ are obtained every 11 s, during hours of continuous observations, tracking numbers of bright stars. SSS is a reliable, transportable instrument based on sound theory, carefully tested, allowing calibrated $C_n^2$ and wind velocity profiles from the ground up to 25 km.

## (c) Contribution to atmospheric knowledge

The use of multi-dimensional analysis of scintillation led to the Scidar class of instruments, allowing the simultaneous determination of vertical profiles of optical turbulence, wind velocity and wind dispersion. These parameters can be obtained under night clear air propagation, with a short time resolution of about 10 s and a vertical resolution of about 300 m, from the ground level up to 25–30 km.

Evidence of the multi-layered structure of the atmosphere was demonstrated during the early 1970s thanks to the multi-dimensional approach, confirming balloon measurements [31]. This is

of major importance, since we should no longer assume that atmospheric turbulence is moving at a constant velocity.

The Scidar technique is well suited to follow the temporal evolution of the wind speed within each turbulent layer, with a time resolution of approximately 10 s. The wind dispersion estimations can also be interpreted in terms of the horizontal wind velocity spectrum in the buoyancy range, as shown in [84]. The authors believe that the use of a faster correlator will enable us to experimentally sample the buoyancy range for length scales ranging from 100 m to several tens of thousands of metres.

Coulman *et al.* [86] have estimated the outer scale of turbulence using $C_n^2$ from Scidar and the gradient of the mean temperature estimated using balloon measurements and found its values to be in the range from 0.5 to 5 m.

Scidar data have also been used in GW studies for characterization of associated turbulence [87–89].

## 5. Satellite stellar scintillation measurements

### (a) Introductory notes

Stellar scintillation from space through the Earth's atmosphere is observed in limb-viewing geometry (figure 3*a*). These observations have special characteristics: first, an observer is located far beyond the atmosphere, and second, the influence of the denser atmospheric layers below the perigee point of the line of sight is eliminated naturally. This distance leads to a substantial enhancement of scintillation during the free-space propagation. As a result, the observed fluctuations of the light flux have relatively large amplitudes even in the case of very weak perturbations of the air density (an example of scintillation records is shown in figure 3*b*). The second feature is also favourable for studying air density variations at high altitudes that are not exploitable from the Earth's ground because of the masking effect of the dense and turbulent boundary layer.

Measurements conducted from space through the Earth's atmosphere bear a certain similarity to ground-based astronomical observations of scintillation of the stars during their occultation by planets [90–93]. However, the large distance between the observer on the Earth and the planet results in a limited spatial resolution, which is of the order of the corresponding Fresnel scale. Even for the planets nearest to the Earth, the spatial resolution is no better than a few hundreds of metres. In observing stars from a low orbiting satellite through the Earth's atmosphere, the Fresnel scale is tens of centimetres.

### (b) Overview of the satellite stellar scintillation measurements of the Earth's atmosphere

First visual observations of stars and planets through the Earth's atmosphere were reported by Russian cosmonauts on board the *Salyut-6* space station. If these scintillations were generated by locally isotropic turbulence with the Kolmogorov spectrum, they should have typical frequencies of a few kilohertz. These scintillations would be impossible to observe with the human eye having a threshold of approximately 10 Hz. The cosmonauts G. Grechko and Yu. Romanenko carried out a set of visual observations of scintillations, where they identified altitudes of noticeable and strong scintillations. Comparison with the scintillation of planets (extended light sources) has shown a significant difference in the altitudes for the observed scintillations. Grechko *et al.* [94] hypothesized that scintillation visually observed from space represents anisotropic 'pancakes' [95], which results from the instability of internal GWs.

The first satellite measurements of stellar scintillations were performed with the human-controlled EFO-1 photometer on board the *Salyut-7* station [96]. The sampling frequency of this photometer was 100 Hz. The analyses of the EFO-1 data have shown that air density irregularities in the stratosphere, between 25 and 35 km, are stretched along the Earth's surface [97]. The anisotropy coefficient was estimated to be over 25 for vertical scales in the range of 0.1–1 km.

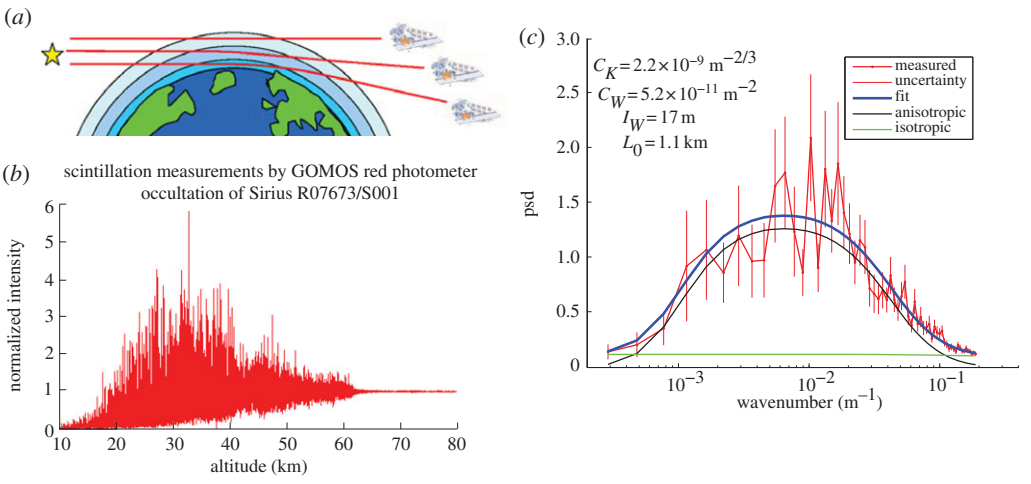


**Figure 3.** (*a*) A schematic of occultation measurements. (*b*) An example of scintillation records by the GOMOS photometers. (*c*) Scintillation spectrum (red) and retrieval results at 33 km altitudes for the occultation of R08738/S002, 12°N 155°E, carried out 1 November 2003, $\alpha = 50^\circ$; blue—the fit with indicated anisotropic (black) and isotropic (green) components of the scintillation spectrum. The values of the retrieved GW and turbulence parameters are also indicated in the figure. (Online version in colour.)

It was found that scintillation spectra have a characteristic vertical scale of about 40–60 m with a rapid decay at smaller scales. Some observations at altitudes of 40–50 km [98] did not reveal this scale. The vertical spectra of temperature fluctuations obtained from scintillation records were in agreement with those derived from direct measurements in the stratosphere for the scales from 50 m to 1 km [99]. For smaller scales, a considerable discrepancy was reported. This was explained by significant changes in the statistical properties of irregularities below some transition scale (approx. 50 m) and by insufficient sampling frequency of EFO-1 and chromatic dispersion in the atmosphere, which prevented reliable studies for these small scales. The main results of 10 years of EFO-1 measurements are summarized in [100].

Great progress in studies of air density irregularities using satellite observations of stellar scintillation has been achieved with the EFO-2 photometer operated on board the Russian *MIR* station in 1996–1999. The human-controlled EFO-2 photometer has a central wavelength of 485 nm and a set of optical filters with various chromatic widths. The sampling frequency was also variable, up to 16 kHz [101]. Despite the limited amount of occultations performed (about 100 within the latitudinal band $\pm 60^\circ$), these scintillation data have allowed the understanding and analysis of statistical and spectral properties of scintillations [68,101] and have validated the scintillation theory developed in [52]. Furthermore, a new approach that allows the solution of the problem of the reconstruction of the three-dimensional spectrum of air density irregularities using one-dimensional scintillation auto-spectra was proposed by Gurvich & Kan [56]. In this approach, the spectrum of the air density irregularities is parametrized, the theoretical relations that connect the three-dimensional spectrum of air density irregularities and the one-dimensional scintillation spectrum at the observation point are deduced, and the parameters of the spectral model are retrieved via fitting experimental scintillation spectra. This method is discussed more in §5*c* and the results of the application of this method to the scintillation measurements by EFO-2 are discussed in §5*d*.

Scintillation data with global coverage became available with the launch of the Global Ozone Monitoring by Occultation of Stars (GOMOS) instrument on board the *Envisat* satellite [102–104]. GOMOS is equipped with two fast photometers, which record the stellar flux synchronously in the blue (473–527 nm, $\lambda_B \approx 500$ nm) and red (646–698 nm, $\lambda_R \approx 672$ nm) wavelength ranges with a sampling frequency of 1 kHz in the limb-viewing geometry. The algorithm for the reconstruction of GW and turbulence spectra parameters has been developed further [20], adapted to the

GOMOS measurements and applied to a large GOMOS dataset [58,105,106]. Several studies have been dedicated to bichromatic scintillations [107–109] and double star occultations [110]. These issues are discussed more below.

## (c) Approaches to data analyses

The method that allows information to be obtained about the parameters of the three-dimensional spectrum of air density irregularities using one-dimensional scintillation spectra was first proposed by Gurvich & Kan [56] and then developed further by Gurvich & Chunchuzov [19] and Sofieva *et al*. [20]. In this approach, the spectrum of the air density irregularities is parametrized and the parameters of the spectral model are retrieved via fitting experimental scintillation spectra. Large satellite velocity ensures the validity of the frozen-field approximation. The spectrum $\Phi_\nu$ of refractivity fluctuations is represented as a sum of two statistically independent components, i.e. anisotropic, $\Phi_W$, and isotropic, $\Phi_K$:

$$\Phi_\nu = \Phi_W + \Phi_K. \tag{5.1}$$

For parametrization of the anisotropic component $\Phi_W$, which corresponds to anisotropic irregularities generated by a random ensemble of internal GWs, the spectrum (2.7) has been used in [19,20]. In [56], the analogue of (2.7) but without an outer scale was used. For parametrization of $\Phi_K$, which corresponds to isotropic irregularities generated by turbulence appearing as a result of GW breaking and/or different instabilities of atmospheric motions, the Oboukhov–Corrsin model of locally isotropic turbulence [111] has been used:

$$\left.\begin{aligned} &\Phi_K(\kappa) = 0.033 C_n^2 \kappa^{-11/3} \exp\left(-\left(\frac{\kappa}{\kappa_m}\right)^2\right) \\ \text{and}\quad &\kappa^2 = \kappa_x^2 + \kappa_y^2 + \kappa_z^2, \end{aligned}\right\} \tag{5.2}$$

where $C_n^2$ is the structure characteristic of isotropic fluctuations (related with the structure characteristic of temperature fluctuations as $C_\mathrm{T}^2 = \langle T\rangle^2 C_n^2$) and $\kappa_m$ is the inner scale of isotropic irregularities. The structure characteristic $C_n^2$ is proportional to $\varepsilon_\nu/\varepsilon^{1/3}$, where $\varepsilon_\nu$ is the rate of dissipation of refractivity fluctuations and $\varepsilon$ is the kinetic energy dissipation rate.

Theoretical relations that allow the calculation of a one-dimensional spectrum of relative fluctuations of intensity at the observation plane from the given spectrum of air density irregularities (the forward model) have been developed in [52,56] in the phase screen approximation under the weak scintillation assumption. In the framework of the phase screen approximation, the effect of the extended atmosphere on the light wave passing through it is replaced by that of a virtual thin phase screen. It is assumed that this screen produces the same phase modulation on the propagated waves as the extended atmosphere [16].

The spectral model of refractivity irregularities has altogether six parameters: for the anisotropic component, they are the structure characteristic $C_W$, the anisotropy coefficient $\eta$, the inner scale $l_W$ and the outer scale $L_0$; for the isotropic component, they are the structure characteristic $C_n^2$ and the Kolmogorov scale $l_\mathrm{K}$. However, not all of them can be retrieved from scintillation spectra. Numerical simulations [52] have shown that the anisotropy coefficient cannot be estimated from scintillation spectra, except for very oblique occultations. The Kolmogorov scale can be retrieved from scintillation measurements only with sufficient (greater than 10 kHz) sampling frequency of the photometer, and only if it is larger than the Fresnel scale. This was possible with the *MIR* photometer having the maximal sampling frequency of 16 kHz (the vertical resolution is a few decimetres), but impossible with the GOMOS sampling frequency of 1 kHz photometer (the vertical resolution is about 1 m). Thus, it was possible to retrieve five parameters of refractivity spectra from *MIR* scintillations, and four parameters from the GOMOS measurements. Typical values for the non-retrieved parameters, i.e. the anisotropy coefficient $\eta = 30$ and the mean value $l_\mathrm{K} = 0.25$ m for the Kolmogorov scale [57], have been used in retrievals [20]. The detailed description of the algorithm for reconstruction of GW and turbulence

spectra parameters is presented in [20]. The inversion procedure is based on a nonlinear fitting of the experimental scintillation spectra by the modelled ones. An example of the experimental scintillation spectrum and the retrieval results is shown in figure 3*c*. The developed algorithm is rather fast, and thus it is suitable for processing of vast amounts of satellite data.

The turbulent structure characteristic $C_n^2$ (or $C_T^2$) can be reconstructed from scintillation data without solving the inverse problem described above, as the scintillation variance corresponding to the isotropic component $\sigma_{I,iso}^2$ is proportional to $C_n^2$. The value of $\sigma_{I,iso}^2$ can be estimated using the simplified spectral analysis, as described in [58,105]. This technique uses the fact that scintillation spectra at scales from $l_W$ to the scale corresponding to the Nyquist frequency are defined mainly by the turbulent component and they are nearly flat.

When chromatic scintillation measurements are available, additional information can be obtained using the cross-spectra and coherence spectra. Details of these analyses and their application to GOMOS data are discussed in [108,109].

## (d) Geophysical results

The scintillation measurements with the EFO-2 photometer on board the *MIR* station have provided estimates of GW and turbulence spectra parameters for altitudes of 25–70 km [57] for the first time, as these altitudes are very difficult to explore with other methods having comparable vertical resolution. Typical values of the parameters and their altitude dependence have been obtained. It was found that the Kolmogorov scale $l_K$ increases monotonically with height from a few decimetres at altitudes of 27–30 km to 1–1.5 m at 63–67 km. The inner scale of the anisotropic component $l_W$ (proportional to the buoyancy scale) increases more rapidly from 1–2 m at altitudes of 27–30 km to 10–30 m at 45–53 km. Between the scales $l_K$ and $l_W$, there is a scale range whose width increases with height. The retrieved estimates of the structure characteristic of the anisotropic component $C_W$ for altitudes of 27–53 km are found to be in good agreement with predictions based on the assumption that the regime of saturated internal GWs exists within this altitude range [22,112]. The estimates of the turbulent structure characteristic $C_T^2$ increase almost exponentially with height from $(2\text{–}10) \times 10^{-5}\,\mathrm{K^2\,m^{-2/3}}$ at 27–30 km to $(0.5\text{–}2) \times 10^{-2}\,\mathrm{K^2\,m^{-2/3}}$ at 65–67 km. For altitudes of 60–67 km, these estimates are in agreement with *in situ* measurements [113].

The retrieved Kolmogorov scales allow for the estimation of the rate of kinetic energy dissipation $\varepsilon$ to heat. For the heights 60–67 km, the obtained values $\varepsilon = (1\text{–}5) \times 10^{-3}\,\mathrm{m^2\,s^{-3}}$ agree with the results of *in situ* measurements [113]. As altitude decreases, the dissipation rate decreases monotonically to $(0.5\text{–}10) \times 10^{-7}\,\mathrm{m^2\,s^{-3}}$ at 27–30 km. The simultaneous measurements of $\varepsilon$ and $C_T^2$ have allowed for the estimation of the dissipation rate of air density irregularities through molecular diffusion. The calculated height dependence of the Bolgiano–Oboukhov scale [111] has shown that the assumption (used in the model) of local isotropy of small-scale irregularities is certainly justified above 35 km.

The *MIR* scintillation data have also allowed for the retrievals of the outer scale of the anisotropic component [19] and for the detection of quasi-periodic disturbances in atmospheric air density and temperature [114].

Observations of stellar scintillations by GOMOS have confirmed the estimates of GW and turbulence spectra parameters obtained from *MIR*. Furthermore, the global coverage of GOMOS measurements has allowed for the study of spatio-temporal distributions of these parameters, including the polar regions. Already, first analyses have shown surprising results. Strong increases in scintillation variance and $C_T^2$ at high latitudes in winter were observed [58,105]. It was shown that the maximum of these enhancements can be associated with the polar night jet. The simplified spectral analysis has shown the transition of scintillation variance towards small scales with altitude, which is probably related with turbulence appearing as a result of wave breaking. The breaking of GWs in the polar night jet seems to start in the upper stratosphere. This previously predicted feature [115,116] was confirmed by the GOMOS observations for the first time.

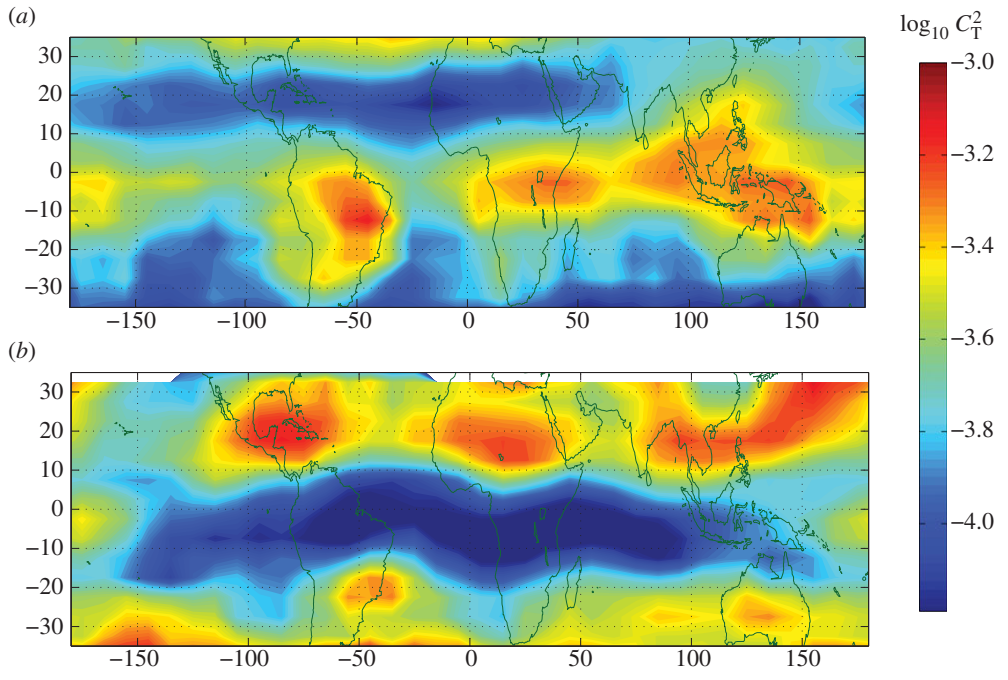


**Figure 4.** $C_T^2$ map showing ($K^2\ m^{-2/3}$) at 42 km for (*a*) January–March, December and for (*b*) June–September, logarithmic colour scale. The data are averaged in 5 × 10° latitude–longitude bins and a three-point smoothing is applied to the obtained fields. Adapted from [58]. (Online version in colour.)

In [58], the first estimation of global distribution of $C_T^2$ at altitudes of 30–50 km for the four seasons of year 2003 is presented. As a general rule, the values of zonal mean $C_T^2$ increase with altitude. The largest $C_T^2$ values are achieved in polar regions in winter, where they may reach $0.006\ K^2\ m^{-2/3}$ in the Southern Hemisphere, i.e. values that are comparable with those observed in the turbulent boundary layer (fig. 2 in [58]). Weaker turbulence is observed at low latitudes. Minimal values of $C_T^2$ are less than $10^{-4}\ K^2\ m^{-2/3}$ there and it has a pronounced zonal structure. The average turbulence intensity at altitudes of approximately 42 km follows the sub-solar point, with enhancements located mainly over continents (figure 4, note that uncertainty of the estimate is much smaller than their variability). Turbulence enhancements in tropical regions are not related with orography. Despite a good correlation with typical regions of deep convection, the overall distribution of $C_T^2$ displays a more complicated structure.

GW spectra parameters at altitudes of 30–50 km observed in 2003 are discussed in detail in [106], where their global distributions are presented. The use of outer scale estimations has enabled the estimation of an important GW parameter, the potential energy $E_P$ per unit mass [106]. Enhancements of $E_P$ in equatorial regions are clearly observed, analogous to those found in global analysis of radio-occultation data. They are caused by large values of GW outer scale at these locations. Enhanced $E_P$ is observed also in the Southern Hemisphere winter at high latitudes, but there is no symmetric $E_P$ enhancement in the Northern Hemisphere winter at high latitudes. Sofieva *et al.* [106] suggested that it is probably caused by the fact that occultations at Northern Hemisphere winter high latitudes were carried out in January and in December 2003, when sudden stratospheric warmings (SSW) lasted a significant part of the observational period. It coincides with previous lidar observations [117], which have shown reduced GW activity during SSW.

## (e) Perspectives and discussion

Related to GOMOS measurements, future multi-year analysis of GOMOS scintillation measurements will refine the observations and will provide information about spatial and

inter-annual variability of GW and turbulence spectra parameters in the stratosphere. So far, the retrievals have been performed in the altitude range 30–50 km. The upper altitude for parameter reconstruction is limited by the scintillation strength: usually the scintillations significantly exceed instrumental noise below 50 km in occultations of stars that are brighter than visual magnitude 1.6 for GOMOS. Sometimes, the amplitude of scintillation is large enough also at altitudes greater than 50 km. In such cases, the retrievals of the parameters of the spectral model can be performed at higher altitudes, up to 70 km. The lower limit is dictated by the weak scintillation assumption used in the forward model. The analysis [67] has shown that the parameters of the three-dimensional spectra of stratospheric irregularities can be retrieved under conditions of relatively strong scintillation. However, computing the scintillation spectra for strong scintillation requires rather heavy numerical calculations, which are hardly compatible with an iterative nonlinear fitting procedure, for application to the vast amount of satellite data.

Since the satellite measurements are indirect, information about the structure of air density irregularities is feasible only with the assumption on their spatial spectra. The choice of the spectral model used in the analyses of *MIR* and GOMOS data was dictated by the requirement to contain all the important physical parameters controlling the scintillation spectra, on the one hand, and the simplicity of computing the scintillation spectra, on the other. Although the three-dimensional spectral model of atmospheric irregularities is more complicated (a newly developed spectrum with the variable anisotropy [28] is definitely more realistic), its application for the interpretation of scintillation measurements is not straightforward and requires first a feasibility and sensitivity study.

Other extensions of GOMOS data analyses can include studying chromatic scintillations as demonstrated in [109] and quasi-periodic disturbances in the atmospheric density and temperature fields, which appear rather often as large peaks on the background of the smooth scintillation spectrum [20,114].

In the GOMOS dataset, there are a few quasi-horizontal occultations, which can potentially provide estimates for the anisotropy coefficient, as discussed in [108]. Other 'specific' GOMOS observations are scintillations of double stars. As was shown in [110], the scintillation spectra of double stars unresolved by the detector, which have close magnitudes, are more complicated (they are modulated), but, at the same time, they are more informative; thus they can provide potentially additional information about parameters of the atmospheric fine structure.

## 6. Air-borne measurements of stellar scintillation

The scintillation of stars observed through the Earth's atmosphere was also reported from balloon-borne investigation of the nocturnal vertical distribution of stratospheric minor constituents [118]. Compared with satellite observations of stellar scintillation, the geometry (and the physics) is very similar, but the relative velocity of the line of sight with respect to the atmosphere is of the order of $10\,\mathrm{m\,s^{-1}}$ or less while it exceeds $1\,\mathrm{km\,s^{-1}}$ for the satellite observations. Consequently, the small-scale fluctuations are much easier to observe and characterize from a balloon-borne instrument. The altitude range where scintillation can be analysed is practically contiguous—or slightly overlapping—thus allowing the observation of the whole stratosphere. While the analysis of satellite measurements is currently limited to altitudes above 30 km by the strong scintillation, the balloon-borne observations are limited upwards by their maximal float altitude, around 30–40 km. In the case of satellite measurements, the distance between the observing instrument and the dominant refractivity fluctuations is large (approx. 3200 km for GOMOS) and does not change significantly with the altitude of the ray perigee. For balloon-borne observations, this distance increases from zero up to 400–500 km when the tangent point decreases from the float altitude down to the troposphere.

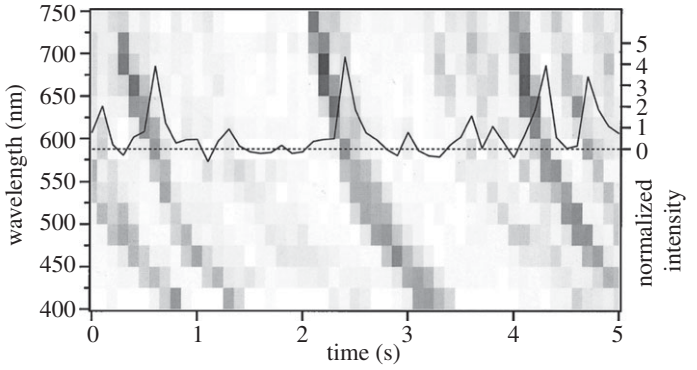


**Figure 5.** Relative flux enhancements as a function of time for 14 chromatic channels (left axis). The grey scale ranges from 0 (white) to 10 (black), thus dark pixels correspond to larger intensity. The series of relative intensity is shown on the right-hand axis for channel 8 (575–600 nm). Adapted from [119].

During the preparation of the GOMOS instrument, a balloon-borne experiment especially dedicated to the multi-spectral recording of scintillation, AMON-RA, was performed in February 1999 and analysed [119]. The results of this balloon experiment allowed for the validation of the hypothesis and parameters underlying the scintillation correction used during the GOMOS data processing. The fact that the characteristic scintillation frequencies recorded from a balloon-borne gondola are much smaller than from a satellite allowed the scintillation to be recorded simultaneously with 10 Hz sampling frequency and within 14 spectral channels covering the full visible range (see figure 5, adapted from [119]). The observed intensity peaks—light focusing—produced by small-scale refractivity fluctuations are observed at all wavelengths, but with slightly different arrival times because of the refractive dispersion. Since the refraction angle is nearly proportional to the refractivity, the shape of these peaks reproduces the wavelength dependence of standard air refractivity [120].

The experiment AMON-RA was flown again in March 2003 during an *Envisat* (and thus GOMOS) validation campaign [21]. The duration of continuous recording was extended from 60 to 600 s, thus allowing easier and deeper statistical and spectral analysis of the scintillation time series. In order to retrieve the spectral parameters of the small-scale atmospheric dynamics, an analytical formulation of the two-dimensional scintillation spectra was developed. This spectral model is fully compatible with the model used for the analysis of the GOMOS scintillation (see §6) except that the layered structure of the atmosphere is explicitly taken into account, with values of the local parameters variable with the altitude. This analytic model can also handle the case where the light source is at a finite distance (including within the atmosphere) from the observing instrument. This analytic model needs to be numerically integrated in order to be compared with experimental data.

The statistical distribution of recorded intensities follows closely the lognormal model when the scintillation is weak, as expected. Progressive divergence appears when the scintillation becomes moderate, while strong scintillation seems to follow a decreasing exponential law. The intensity distribution is independent of wavelength for the weak scintillation regime. The time spectra of the recorded scintillation are in agreement with the analytic model, and the position of the cut-off allows one to estimate the characteristic inner scale of the anisotropic fluctuations 10–20 m, in general agreement with values deduced (at higher altitudes) from satellite measurements. Finally, the normalized intensity variance closely follows the values predicted by the model, except for the strong scintillation case, where the model is known to be inaccurate and where the chromatic refraction smoothing should be taken into account.

The description and analysis of the scintillation recorded from a stratospheric balloon is qualitatively comparable to the case of the satellite measurements. However, some parameters describing the geometry or characteristic velocities of these measurements are significantly

different, thus allowing exploration of different ranges for altitudes or model parameters. As usual, when comparing local measurements with satellite ones, the global coverage and long-period monitoring capabilities of satellite observations are unique characteristics that also apply to scintillation measurements. One of the potential applications of such experiments might be using them for validation purposes.

## 7. Summary and discussion

The scintillations observed through the Earth's atmosphere result from interaction of light waves and the turbulent atmosphere, thus carrying important information about small-scale processes in the atmosphere. The scintillation can be observed in different viewing geometries, when the line of sight is nearly vertical (ground-based astronomical observations) or nearly horizontal (occultation geometry). Since the scintillation measurements belong to remote sensing measurements, inverse problems are required in order to get information about atmospheric turbulence. The data analyses rely on using spectral models of air density (hence, refractivity) fluctuation, the theory of wave propagation in random media and the inverse problem in order to retrieve some parameters of the spectral model.

There are several limitations and specific features inherent in the scintillation method. For interpretation of scintillations, a spectral model of air density irregularities should be assumed. This model need not necessarily be a comprehensive model of atmospheric dynamics. For good agreement with observed scintillations, it is sufficient to use a model with important (and meaningful) parameters. This model can even be partly or completely empirical. The analyses of the scintillation data provide the values (and variability) of the parameters in different atmospheric conditions. These values may be used in order to evaluate models of atmospheric dynamics and validate different hypotheses.

An important limitation of scintillations as an investigation tool for atmospheric dynamics is that they are insensitive to some parameters of the spectral model (e.g. ground-based scintillation measurements are insensitive to anisotropic irregularities; in the case of satellite stellar occultation measurements, the change of anisotropy is not important for scintillation if the anisotropy is large).

When comparing the parameters retrieved from scintillations with other kinds of measurements, it is important to take into account that the scintillations provide 'effective' parameters, which are averaged along a ray, with the weight function determining the effective region of interaction between the light wave and the turbulent atmosphere.

Stellar scintillation measurements in occultation geometry are characterized by a good spatial resolution, which is limited by the Fresnel scale or by the scale corresponding to the sampling rate of the detector. This also imposes a limitation: information at scales smaller than the Fresnel scale becomes unavailable even with a sufficient sampling rate of the detector.

Nowadays, scintillations have provided useful information about turbulence in the atmosphere from the ground to the mesosphere. The Scidar technique has become a standard experiment for remote sensing of the Earth's atmosphere. Satellite observations of stellar scintillation provide information about the structure of air density irregularities in the altitude range of 25–50 km, where other measurements at such small scales are very scarce. The important strength of scintillations in occultation geometry is that the wavenumber range of the transition of the GW spectrum to turbulence is covered. This opens up the possibility for monitoring GW breaking in the stratosphere. The scintillation is affected by small vertical scale GW (with vertical scales from a few metres to a few kilometres), which are of high importance for parametrization of GW effects in global circulation and climate models. Perhaps the most valuable application of the turbulence parameters retrieved from scintillation measurements is using them to optimize the turbulence schemes in atmospheric models. This becomes increasingly important due to their tendency to higher altitudes and smaller scales.

The authors thank A. S. Gurvich and V. Kan for their help in preparation of this review and for discussions related to stellar scintillations. The work of V. F. Sofieva was supported by the Academy of Finland.

## References


1. Tricot J. (transl.) 1990 *Aristote, Traité du ciel suivi du traité pseudo-aristotélicien du monde*. Translated and with notes by J Tricot. Paris, France: J Vrin.
2. Richter JP. 1970 *The notebooks of Leonardo da Vinci, II*. New York, NY: Dover.
3. Gino MC. 2001 Starry night: the study of stellar scintillation. See http://www.astrophys-assist.com/educate/starry/starrynight.htm.
4. Newton I. 1704 *Opticks or a treatise of the reflections, refractions, inflections and colours of light*. London, UK: S Smith and B Walford.
5. Arago F. 1845 *Leçons d'Astronomie*, 4th edn. Paris, France: Chamerot.
6. Monaco G. 1990 Lorenzo Respighi and star scintillation. *Mem. Soc. Astron. Ital.* **61**, 819–827.
7. Dufour C. 1856 Sur la scintillation des étoiles. *Bulletin de la Société Vaudoise des Sciences Naturelles*, January, pp. 1–10.
8. Montigny C. 1855 Essai sur les effets de la réfraction et de la dispersion produits par l'air atmosphérique. *Mem. Cl. Soc. Acad. R. Belg.* **26**, 1–70.
9. Montigny C. 1856 Sur la scintillation. *Cosmos* **19**, 166–168, 191–196.
10. Montigny C. 1870 Notice sur la séparation des trajectoires décrites dans l'atmosphère par des rayons de même origine sidérale, mais de réfrangibilité différente, et sur les effets de cette séparation à l'égard de la scintillation. *Bull. Acad. R. Belg.* **29**, 88–99.
11. Wolf C. 1868 Sur la scintillation des étoiles. *Comptes Rendus* **LXVI**, 1051.
12. Respighi L. 1872 Sur la scintillation des étoiles. *C. R. Assoc. Fr. Avance. Sci.* **1**, 148–155.
13. Edlen B. 1966 The refractive index of air. *Metrologia* **2**, 71–80. (doi:10.1088/0026-1394/2/2/002)
14. Birch KP, Downs MJ. 1993 An updated Edlén equation for the refractive index of air. *Metrologia* **30**, 155–162. (doi:10.1088/0026-1394/30/3/004)
15. Tatarskii VI. 1971 *The effects of the turbulent atmosphere on wave propagation*. Jerusalem, Israel: Israel Program for Scientific Translations.
16. Ishimaru A. 1978 *Wave propagation and scattering in random media*, vol. 2. New York, NY: Academic.
17. Kraichnan RH. 1974 On Kolmogorov's inertial-range theories. *J. Fluid Mech.* **62**, 305–330. (doi:10.1017/S002211207400070X)
18. Frish U. 1995 *Turbulence: the legacy of A. N. Kolmogorov*. Cambridge, UK: Cambridge University Press.
19. Gurvich AS, Chunchuzov IP. 2005 Estimates of characteristic scales in the spectrum of internal waves in the stratosphere obtained from space observations of stellar scintillations. *J. Geophys. Res.* **110**, D03114. (doi:10.1029/2004JD005199)
20. Sofieva VF, Gurvich AS, Dalaudier F, Kan V. 2007 Reconstruction of internal gravity wave and turbulence parameters in the stratosphere using GOMOS scintillation measurements. *J. Geophys. Res.* **112**, D12113. (doi:10.1029/2006JD007483)
21. Robert C, Conan JM, Michau V, Renard JB, Dalaudier F. 2008 Retrieving parameters of the anisotropic refractive index fluctuations spectrum in the stratosphere from balloon-borne observations of stellar scintillation. *J. Opt. Soc. Am. A* **25**, 379–392. (doi:10.1364/JOSAA.25.000379)
22. Smith SA, Fritts DC, VanZandt TE. 1987 Evidence of a saturation spectrum of atmospheric gravity waves. *J. Atmos. Sci.* **44**, 1404–1410. (doi:10.1175/1520-0469(1987)044<1404:EFASSO>2.0.CO;2)
23. Fritts DC, Alexander MJ. 2003 Gravity wave dynamics and effects in the middle atmosphere. *Rev. Geophys.* **41**, 1003. (doi:10.1029/2001RG000106)
24. Chunchuzov IP. 2002 On the high-wavenumber form of the Eulerian internal wave spectrum in the atmosphere. *J. Atmos. Sci.* **59**, 1753–1772. (doi:10.1175/1520-0469(2002)059<1753:OTHWFO>2.0.CO;2)
25. Nastrom GD, Gage KS. 1985 A climatology of atmospheric wavenumber spectra of wind and temperature observed by commercial aircraft. *J. Atmos. Sci.* **42**, 950–960. (doi:10.1175/1520-0469(1985)042<0950:ACOAWS>2.0.CO;2)

26. Cho NJY, Zhu Y, Newell RE, Anderson BE, Barrick JD, Gregory GL, Sachse GW, Carroll MA, Albercook GM. 1999 Horizontal wavenumber spectra of winds, temperature, and trace gases during the Pacific Exploratory Missions: 1. Climatology. *J. Geophys. Res.* **104**, 5697–5716. (doi:10.1029/98JD01825)
27. Bacmeister JT, Eckermann SD, Newman PA, Lait L, Chan KR, Loewenstein M, Proffitt MH, Gary BL. 1996 Stratospheric horizontal wavenumber spectra of winds, potential temperature, and atmospheric tracers observed by high-altitude aircraft. *J. Geophys. Res.* **101**, 9441–9470. (doi:10.1029/95JD03835)
28. Gurvich AS, Chunchuzov IP. 2008 Three-dimensional spectrum of temperature fluctuations in stably stratified atmosphere. *Ann. Geophys.* **26**, 2037–2042. (doi:10.5194/angeo-26-2037-2008)
29. Dalaudier F, Gurvich AS. 1997 A scalar three-dimensional spectral model with variable anisotropy. *J. Geophys. Res.* **102**, 19 449–19 459. (doi:10.1029/97JD00962)
30. Gurvich AS. 1997 A heuristic model of three-dimensional spectra of temperature inhomogeneities in the stably stratified atmosphere. *Ann. Geophys.* **15**, 856–869. (doi:10.1007/s00585-997-0856-x)
31. Vernin J, Roddier F. 1973 Experimental determination of two-dimensional spatiotemporal power spectra of stellar light scintillation. Evidence for a multilayer structure of the air turbulence in the upper troposphere. *J. Opt. Soc. Am.* **63**, 270–273. (doi:10.1364/JOSA.63.000270)
32. Azouit M, Vernin J, Barletti R, Ceppatelli G, Righini A, Speroni N. 1980 Remote sensing of atmospheric turbulence by means of a fast optical method: a comparison with simultaneous *in situ* measurements. *J. Appl. Meteorol.* **19**, 834–838. (doi:10.1175/1520-0450(1980)019<0834:RSOATB>2.0.CO;2)
33. Dalaudier F, Sidi C, Crochet M, Vernin J. 1994 Direct evidence of 'sheets' in the atmospheric temperature field. *J. Atmos. Sci.* **51**, 237–248. (doi:10.1175/1520-0469(1994)051<0237:DEOITA>2.0.CO;2)
34. Luce H, Crochet M, Dalaudier F, Sidi C. 1995 Interpretation of VHF ST radar vertical echoes from *in situ* temperature sheet observations. *Radio Sci.* **30**, 1003–1025. (doi:10.1029/95RS00713)
35. Coulman CE, Vernin J, Fuchs A. 1995 Optical seeing: mechanism of formation of thin turbulent laminae in the atmosphere. *Appl. Opt.* **34**, 5461–5474. (doi:10.1364/AO.34.005461)
36. Lovejoy S, Tuck AF, Hovde SJ, Schertzer D. 2008 Do stable atmospheric layers exist? *Geophys. Res. Lett.* **35**, L01802. (doi:10.1029/2007GL032122)
37. Lovejoy S, Schertzer D, Allaire V, Bourgeois T, King S, Pinel J, Stolle J. 2009 Atmospheric complexity or scale by scale simplicity? *Geophys. Res. Lett.* **36**, L01801. (doi:10.1029/2008GL035863)
38. Lovejoy S, Schertzer D. 2010 Towards a new synthesis for atmospheric dynamics: space time cascades. *Atmos. Res.* **96**, 1–52. (doi:10.1016/j.atmosres.2010.01.004)
39. Zilitinkevich SS, Elperin T, Kleeorin N, Rogachevskii I. 2007 Energy- and flux-budget (EFB) turbulence closure model for stably stratified flows. I. Steady-state, homogeneous regimes. *Bound.-Layer Meteorol.* **125**, 167–191. (doi:10.1007/s10546-007-9189-2)
40. Zilitinkevich SS, Elperin T, Kleeorin N, Rogachevskii I, Esau I, Mauritsen T, Miles MW. 2008 Turbulence energetics in stably stratified geophysical flows: strong and weak mixing regimes. *Q. J. R. Meteorol. Soc.* **134**, 793–799. (doi:10.1002/qj.264)
41. Zilitinkevich SS, Elperin T, Kleeorin N, L'vov V, Rogachevskii I. 2009 Energy- and flux-budget turbulence closure model for stably stratified flows. II. The role of internal gravity waves. *Bound.-Layer Meteorol.* **133**, 139–164. (doi:10.1007/s10546-009-9424-0)
42. Sukoriansky S, Galperin B, Staroselsky I. 2005 A quasinormal scale elimination model of turbulent flows with stable stratification. *Phys. Fluids* **17**, 085107. (doi:10.1063/1.2009010)
43. Sukoriansky S, Galperin B, Perov V. 2006 A quasi-normal scale elimination model of turbulence and its application to stably stratified flows. *Nonlin. Process. Geophys.* **13**, 9–22. (doi:10.5194/npg-13-9-2006)
44. Sukoriansky S, Galperin B. 2008 Anisotropic turbulence and internal waves in stably stratified flows (QNSE theory). *Phys. Scripta* **T132**, 014036. (doi:10.1088/0031-8949/2008/T132/014036)
45. Tatarskii VI. 1961 *Wave propagation in a turbulent medium*. New York, NY: McGraw-Hill.
46. Uscinski BJ. 1977 *The elements of wave propagation in random media*. New York, NY: McGraw-Hill.

47. Rytov SM, Kravtsov YA, Tatarskii VI. 1989 *Principles of statistical radiophysics*. Berlin, Germany: Springer.
48. Andrews LC, Phillips RL. 2005 *Laser beam propagation through random media*. Bellingham, WA: SPIE.
49. Haugstad BS. 1978 Effects of inhomogeneous background on radiation propagating through turbulent planetary atmospheres. *Radio Sci.* **13**, 435–440. (doi:10.1029/RS013i003p00435)
50. Hubbard WB, Jokipii JR, Wilking BA. 1978 Stellar occultation by turbulent planetary atmospheres: a wave-optical theory including a finite scale height. *Icarus* **34**, 374–395. (doi:10.1016/0019-1035(78)90174-4)
51. Hinson DP. 1986 Strong scintillation during atmospheric occultations: theoretical intensity spectra. *Radio Sci.* **21**, 257–270. (doi:10.1029/RS021i002p00257)
52. Gurvich AS, Brekhovskikh V. 2001 A study of turbulence and inner waves in the stratosphere based on the observations of stellar scintillations from space: a model of scintillation spectra. *Waves Random Media* **11**, 163–181. (doi:10.1080/13616670109409781)
53. Dravins D, Lindegren L, Mezey E, Young AT. 1997 Atmospheric intensity scintillation of stars. I. Statistical distributions and temporal properties. *Publ. Astron. Soc. Pac.* **109**, 173–207. See http://www.jstor.org/stable/40680883.
54. Dravins D, Lindegren L, Mezey E, Young AT. 1997 Atmospheric intensity scintillation of stars. II. Dependence on optical wavelength. *Publ. Astron. Soc. Pac.* **109**, 725–737. See http://www.jstor.org/stable/40680954.
55. Dravins D, Lindegren L, Mezey E, Young AT. 1998 Atmospheric intensity scintillation of stars. III. Effects for different telescope apertures. *Publ. Astron. Soc. Pac.* **110**, 610–633. (doi:10.1086/316161)
56. Gurvich AS, Kan V. 2003 Structure of air density irregularities in the stratosphere from spacecraft observations of stellar scintillation: 1. Three-dimensional spectrum model and recovery of its parameters. *Izv. Atmos. Oceanic Phys.* **39**, 300–310.
57. Gurvich AS, Kan V. 2003 Structure of air density irregularities in the stratosphere from spacecraft observations of stellar scintillation: 2. Characteristic scales, structure characteristics, and kinetic energy dissipation. *Izv. Atmos. Oceanic Phys.* **39**, 311–321.
58. Gurvich AS, Sofieva VF, Dalaudier F. 2007 Global distribution of CT2 at altitudes 30–50 km from space-borne observations of stellar scintillation. *Geophys. Res. Lett.* **34**, L24813. (doi:10.1029/2007GL031134)
59. Shishov VI. 1968 Theory of wave propagation in random media. *Izv. VU Radiofiz. Z.* **11**, 866–875, L24813. (doi:10.1029/2007GL031134)
60. Fante RL. 1981 Two-position, two-frequency mutual-coherence function in turbulence. *J. Opt. Soc. Am.* **71**, 1446–1451. (doi:10.1364/JOSA.71.001446)
61. Uscinski BJ. 1985 Analytical solution of the fourth-moment equation and interpretation as a set of phase screens. *J. Opt. Soc. Am.* **2**, 2077–2091. (doi:10.1364/JOSAA.2.002077)
62. Dashen R. 1979 Path integrals for waves in random media. *J. Math. Phys.* **20**, 894–920. (doi:10.1063/1.524138)
63. Codona JL, Creamer DB, Flatté SM, Frehlich RG, Henyey FS. 1986 Solution for the fourth moment of waves propagating in random media. *Radio Sci.* **21**, 929–948. (doi:10.1029/RS021i006p00929)
64. Martin JM, Flatté SM. 1988 Intensity images and statistics from numerical simulation of wave propagation in three-dimensional random media. *Appl. Opt.* **27**, 2111–2126. (doi:10.1364/AO.27.002111)
65. Filinov VS. 1995 Monte Carlo simulation in the theory of wave propagation in random media: II. Scintillation index, second and fourth moments. *Waves Random Media* **5**, 277–287. (doi:10.1088/0959-7174/5/3/002)
66. Shishov VI. 1971 Diffraction of waves by a strongly refracting random phase screen. *Radiophys. Quant. Electron.* **14**, 70–75. (doi:10.1007/BF01032910)
67. Gurvich AS, Vorob'ev VV, Fedorova OV. 2006 Determination of parameters of the spectrum of internal waves in the stratosphere from space-based observations of strong stellar scintillation. *Izv. Atmos. Oceanic Phys.* **42**, 463–473. (doi:10.1134/S0001433806040062)
68. Gurvich AS, Kan V, Savchenko SA, Pakhomov AI, Padalka GI. 2001 Studying the turbulence and internal waves in the stratosphere from spacecraft observations of stellar scintillation. II. Probability distributions and scintillation spectra. *Izv. Atmos. Oceanic Phys.* **37**, 452–465.
69. Gorbunov ME. 1996 Three-dimensional satellite refractive tomography of the atmosphere: numerical simulation. *Radio Sci.* **31**, 95–104. (doi:10.1029/95RS01353)

70. Roddier F. 1981 The effects of atmospheric turbulence in optical astronomy. *Prog. Opt.* **19**, 281–376. (doi:10.1016/S0079-6638(08)70204-X)
71. Mikesell AH. 1955 *The scintillation of starlight*. Publications of the United States Naval Observatory, Second Series, vol. 17, part 4. Washington, DC: U.S. Government Printing Office.
72. Protheroe WM. 1964 The motion and structure of stellar shadow-band patterns. *Q. J. R. Meteorol. Soc.* **90**, 27–42. (doi:10.1002/qj.49709038304)
73. Young AT. 1967 Photometric error analysis. VI. Confirmation of Reiger's theory of scintillation. *Astron. J.* **72**, 747. (doi:10.1086/110303)
74. Rocca A, Roddier F, Vernin J. 1974 Detection of atmospheric turbulent layers by spatiotemporal and spatioangular correlation measurements of stellar-light scintillation. *J. Opt. Soc. Am.* **64**, 1000–1004. (doi:10.1364/JOSA.64.001000)
75. Vernin J, Roddier F. 1975 Détection au sol de la turbulence stratosphérique par intercorrélation spatioangulaire de la scintillation stellaire. *C.R. Acad. Sci. Paris B Sci. Phys.* **280**, 463–465.
76. Caccia JL, Vernin J, Azouit M. 1988 Structure function $C_n^2$ profiling by two-color stellar scintillation with atmospheric dispersion. *Appl. Opt.* **27**, 2229–2235. (doi:10.1364/AO.27.002229)
77. Rocca A, Roddier F, Vernin J. 1974 Detection of atmospheric turbulent layers by spatiotemporal and spatioangular correlation measurements of stellar-light scintillation. *J. Opt. Soc. Am.* **64**, 1000–1004. (doi:10.1364/JOSA.64.001000)
78. Avila R, Vernin J, Masciadri E. 1997 Whole atmospheric-turbulence profiling with generalized scidar. *Appl. Opt.* **36**, 7898–7905. (doi:10.1364/AO.36.007898)
79. Vernin J, Munoz-Tunon C. 1994 Optical seeing at La Palma Observatory. 2: Intensive site testing campaign at the Nordic Optical Telescope. *Astron. Astrophys.* **284**, 311–318.
80. Fuchs A, Tallon M, Vernin J. 1998 Focusing on a turbulent layer: principle of the 'generalized SCIDAR'. *Publ. Astron. Soc. Pac.* **110**, 86–91. (doi:10.1086/316109)
81. Vernin J, Azouit M. 1983 Image processing adapted to the atmosphere speckle. I. Speckle formation in turbulent atmosphere. Statistical properties. *J. Opt.* (*Paris*) **14**, 5–9. (doi:10.1088/0150-536X/14/1/001)
82. Vernin J, Azouit M. 1983 Image processing adapted to the atmospheric speckle. II. Remote sounding of turbulence by means of multidimensional analysis. *J. Opt.* (*Paris*) **14**, 131–142. (doi:10.1088/0150-536X/14/3/001)
83. Caccia JL, Azouit M, Vernin J. 1987 Wind and $C_N^2$ profiling by single-star scintillation analysis. *Appl. Opt.* **26**, 1288–1294. (doi:10.1364/AO.26.001288)
84. Caccia JL, Vernin J. 1990 Wind fluctuation measurements in the buoyancy range by stellar scintillation analysis. *J. Geophys. Res.* **95**, 13 683–13 690. (doi:10.1029/JD095iD09p13683)
85. Habib A, Vernin J, Benkhaldoun Z, Lanteri H. 2006 Single star scidar: atmospheric parameters profiling using the simulated annealing algorithm. *Mon. Not. R. Astron. Soc.* **368**, 1456–1462. (doi:10.1111/j.1365-2966.2006.10235.x)
86. Coulman CE, Vernin J, Coqueugniot Y, Caccia JL. 1988 Outer scale of turbulence appropriate to modeling refractive-index structure profiles. *Appl. Opt.* **27**, 155–160. (doi:10.1364/AO.27.000155)
87. Vernin J, Pelon J. 1986 Scidar/lidar description of a gravity wave and associated turbulence: preliminary results. *Appl. Opt.* **25**, 2874–2877. (doi:10.1364/AO.25.002874)
88. Vernin J, Trinquet H, Jumper G, Murphy E, Ratkowski A. 2007 OHP02 gravity wave campaign in relation to optical turbulence. *Environ. Fluid Mech.* **7**, 371–382. (doi:10.1007/s10652-007-9032-9)
89. Jumper GY, Murphy EA, Ruggiero FH, Roadcap JR, Ratkowski AJ, Vernin J, Trinquet H. 2007 OHP-APT 2002 gravity wave campaign: waves, turbulence and forecasts. *Environ. Fluid Mech.* **7**, 351–370. (doi:10.1007/s10652-007-9030-y)
90. Jokipii JR, Hubbard WB. 1977 Stellar scintillations by turbulent planetary atmospheres: the Beta Scorpii events. *Icarus* **30**, 537–550. (doi:10.1016/0019-1035(77)90107-5)
91. Elliot JL, Veverka J. 1976 Stellar occultation spikes as probes of atmospheric structure and composition. *Icarus* **27**, 359–386. (doi:10.1016/0019-1035(76)90015-4)
92. Hubbard WB, Lellouch E, Sicardy B. 1988 Structure of scintillations in Neptune's occultation shadow. *Astron. J.* **325**, 490–502. (doi:10.1086/166019)

93. Hubbard WB *et al.* 1993 The occultation of 28 Sgr by Titan. *Astron. Astrophys.* **269**, 541–563. See http://adsabs.harvard.edu/full/1993A%26A...269..541H.
94. Grechko GM, Gurvich AS, Romanenko YV. 1980 Structure of stratospheric density irregularities as inferred from the observations on board Salyut 6. *Izv. Akad. Nauk SSSR, Fiz. Atmos. Okeana* **16**, 339–344.
95. Phillips OM. 1967 The generation of clear-air turbulence by the degradation of internal waves. In *Atmospheric turbulence and radio wave propagation* (eds VI Tatarskiy, AM Yaglom), pp. 130–136. Moscow, USSR: Nauka.
96. Gurvich AS, Zakharov I, Kan V, Lebedev VV, Nesterenko AA, Neuzhil L, Pakhomov AI, Savchenko SA. 1985 Stellar scintillations inferred from observations on board the Salyut 7 space station. *Izv. Akad. Nauk SSSR, Fiz. Atmos. Okeana* **21**, 1235–1241.
97. Alexandrov AP, Grechko GM, Gurvich AS, Kan V, Savchenko SA. 1990 Temperature spectra in the stratosphere from observations of star scintillations from space. *Izv. Atmos. Oceanic Phys.* **26**, 1–8.
98. Grechko GM, Gurvich AS, Kan V, Pakhomov AI, Savchenko SA, Serebrov AA. 1993 Observations of stellar scintillations caused by temperature variations at altitudes of 40 to 50 km. *Izv. Akad. Nauk, Fiz. Atmos. Okeana* **29**, 5–10.
99. Dalaudier F, Gurvich AS, Kan V, Sidi C. 1994 Middle stratosphere temperature spectra observed by scintillation and *in situ* techniques. *Adv. Space Res.* **14**, 61–64. (doi:10.1016/0273-1177(94)90116-3)
100. Grechko GM, Gurvich AS, Kan V, Savchenko SA, Pakhomov AI. 2001 Scintillations of star images observed through the atmosphere from onboard Salyut-7 and Mir space stations. *Atmos. Oceanic Opt.* **14**, 1026–1037.
101. Gurvich AS *et al.* 2001 Studying the turbulence and internal waves in the stratosphere from spacecraft observations of stellar scintillation: I. Experimental technique and analysis of the scintillation variance. *Izv. Atmos. Oceanic Phys.* **37**, 436–451.
102. Kyrölä E *et al.* 2004 GOMOS on Envisat: an overview. *Adv. Space Res.* **33**, 1020–1028. (doi:10.1016/S0273-1177(03)00590-8)
103. Bertaux J-L *et al.* 2004 First results on GOMOS/Envisat. *Adv. Space Res.* **33**, 1029–1035. (doi:10.1016/j.asr.2003.09.037)
104. Bertaux J-L *et al.* 2010 Global ozone monitoring by occultation of stars: an overview of GOMOS measurements on ENVISAT. *Atmos. Chem. Phys.* **10**, 12 091–12 148. (doi:10.5194/acp-10-12091-2010)
105. Sofieva VF *et al.* 2007 Global analysis of scintillation variance: indication of gravity wave breaking in the polar winter upper stratosphere. *Geophys. Res. Lett.* **34**, L03812. (doi:10.1029/2006GL028132)
106. Sofieva VF, Gurvich AS, Dalaudier F. 2009 Gravity wave spectra parameters in 2003 retrieved from stellar scintillation measurements by GOMOS. *Geophys. Res. Lett.* **36**, L05811. (doi:10.1029/2008GL036726)
107. Kan V, Dalaudier F, Gurvich AS. 2001 Chromatic refraction with global ozone monitoring by occultation of stars. II. Statistical properties of scintillations. *Appl. Opt.* **40**, 878–889. (doi:10.1364/AO.40.000878)
108. Kan V. 2004 Coherence and correlation of chromatic stellar scintillations in a space-borne occultation experiment. *Izv. Atmos. Oceanic Opt.* **17**, 725–735.
109. Gurvich AS, Dalaudier F, Sofieva VF. 2005 Study of stratospheric air density irregularities based on two-wavelength observation of stellar scintillation by Global Ozone Monitoring by Occultation of Stars (GOMOS) on Envisat. *J. Geophys. Res.* **110**, D11110. (doi:10.1029/2004JD005536)
110. Sofieva VF, Dalaudier F, Kan V, Gurvich AS. 2009 Technical note: scintillations of the double star alpha Cru observed by GOMOS/Envisat. *Atmos. Chem. Phys.* **9**, 8967–8973. (doi:10.5194/acp-9-8967-2009)
111. Monin AS, Yaglom AM. 1975 *Statistical fluid mechanics*, vol. 2. Cambridge, MA: MIT Press.
112. Sidi C, Lefrere J, Dalaudier F, Barat J. 1988 An improved atmospheric buoyancy wave spectrum model. *J. Geophys. Res.* **93**, 774–790. (doi:10.1029/JD093iD01p00774)
113. Lübken F-J, Hillert W, Lehmacher G, Von Zahn U. 1993 Experiments revealing small impact of turbulence on the energy budget of the mesosphere and lower thermosphere. *J. Geophys. Res.* **98**, 20 369–20 384. (doi:10.1029/93JD02055)
114. Gurvich AS, Yakushkin IG. 2004 Spacecraft observations of quasi-periodic structures in the stratosphere. *Izv. Atmos. Oceanic Phys.* **40**, 659–667.

115. Duck TJ, Whiteway JA, Carswell AI. 2001 The gravity wave Arctic stratospheric vortex interaction. *J. Atmos. Sci.* **58**, 3581–3596. (doi:10.1175/1520-0469(2001)058<3581:TGWASV>2.0.CO;2)
116. Jiang JH, Wu DL. 2001 UARS MLS observations of gravity waves associated with the Arctic winter stratospheric vortex. *Geophys. Res. Lett.* **28**, 527–530. (doi:10.1029/2000GL011800)
117. Whiteway JA, Carswell AI. 1994 Rayleigh lidar observations of thermal structure and gravity wave activity in the high Arctic during a stratospheric warming. *J. Atmos. Sci.* **51**, 3122–3136. (doi:10.1175/1520-0469(1994)051<3122:RLOOTS>2.0.CO;2)
118. Renard J-B, Pirre M, Robert C, Moreau G, Huguenin D, Russell III JM. 1996 Nocturnal vertical distribution of stratospheric $O_3$, $NO_2$ and $NO_3$ from balloon measurements. *J. Geophys. Res.* **101**, 28 793–28 804. (doi:10.1029/96JD02012)
119. Renard JB, Dalaudier F, Hauchecorne A, Robert C, Lemaire T, Pirre M, Bertaux J-L. 2001 Measurement of stratospheric chromatic scintillation with the AMON-RA balloonborne spectrometer. *Appl. Opt.* **40**, 4254–4260. (doi:10.1364/AO.40.004254)
120. Dalaudier F, Kan V, Gurvich AS. 2001 Chromatic refraction with global ozone monitoring by occultation of stars. I. Description and scintillation correction. *Appl. Opt.* **40**, 866–877. (doi:10.1364/AO.40.000866)